nature physics

LETTERS

https://doi.org/10.1038/s41567-020-0785-0

Strong optical coupling through superfluid Brillouin lasing

Xin He[1,2], Glen I. Harris[1,2], Christopher G. Baker[1,2*], Andreas Sawadsky[1], Yasmine L. Sfendla[1], Yauhen P. Sachkou[1], Stefan Forstner[1] and Warwick P. Bowen[1]

Brillouin scattering has applications ranging from signal processing[1,2], sensing[3] and microscopy[4] to quantum information[5] and fundamental science[6,7]. Most of these applications rely on the electrostrictive interaction between light and phonons[3,7,8]. Here we show that in liquids optically induced surface deformations can provide an alternative and far stronger interaction. This allows the demonstration of ultralow-threshold Brillouin lasing and strong phonon-mediated optical coupling. This form of strong coupling is a key capability for Brillouin-reconfigurable optical switches and circuits[9,10], for photonic quantum interfaces[11] and to generate synthetic electromagnetic fields[12,13]. While applicable to liquids quite generally, our demonstration uses superfluid helium. Configured as a Brillouin gyroscope[14] this provides the prospect of measuring superfluid circulation with unprecedented precision, and exploring the rich physics of quantum fluid dynamics, from quantized vorticity to quantum turbulence[15,16].

Brillouin scattering is an optomechanical process that couples two optical waves via their interaction with travelling acoustic phonons. In the electrostrictive interaction usually employed, the optical electric field induces strain in a medium, and the generated phonons scatter light between the two optical waves via refractive index changes caused by the medium's photoelasticity. However, high optical powers are typically required to exploit the electrostrictive interaction[3]. This can be alleviated by strongly confining the optical field in a photonic nanostructure[17–21] or through resonant enhancement in an optical cavity. The latter of these approaches has allowed recent demonstrations of ultralow-linewidth lasers[22,23], Brillouin lasing in liquid droplets[8], non-reciprocal optical transport[24], Brillouin gyroscopes[14] and low-noise microwave oscillators[2]. Alternatively, optically induced deformations of the boundary of the medium can be leveraged to provide a Brillouin interaction, with scattering induced by the effective refractive index modulation caused by the deformation. In purpose-engineered solid structures these surface interactions can be made comparable to, or even exceed, the native electrostriction[20,21,25].

Here, we transfer the concept of deformation-induced Brillouin scattering to liquid media, specifically a few-nanometre-thick superfluid helium film that coats the surface of a silica microdisc cavity and couples to its whispering gallery modes (Fig. 1a,b) via perturbation of their evanescent field. Similar to other liquids[26], the superfluid film has an exceedingly weak restoring force, affording a compliant dielectric interface that easily deforms in the presence of optical forces[27,28], as illustrated in Fig. 1c. This offers the potential for very large surface deformations and consequently extreme interaction strengths. We show that it allows radiation-pressure interactions with acoustic phonons that are over two orders of magnitude stronger than have been achieved using electrostriction in similarly sized microcavities[29,30]. These interactions are enhanced by a further order of magnitude by the superfluid fountain pressure, where optical absorption-induced entropy gradients induce superfluid flow[31].

In addition to confining light, the microdisc used in our experiments provides confinement for travelling whispering-gallery-like surface acoustic waves in the superfluid film. These acoustic waves are colocated with the optical whispering gallery modes close to the perimeter of the disc (Fig. 1a) and are a class of third sound[32], which manifests as film thickness fluctuations with a restoring force provided by the van der Waals interaction. They generate an effective refractive index grating that scatters photons between forward- and backward-propagating optical whispering gallery modes, forming a Brillouin optomechanical system. The thin wedge-shaped perimeter of the microdisc (Fig. 1b) is engineered to maximize the optical evanescent field at the location of the acoustic wave[28]. Combined with the colocation of light and acoustic waves, this enhances the achievable radiation-pressure coupling by several orders of magnitude compared with conventional optomechanics experiments previously performed with thin superfluid films[15,27,31].

In the backward Brillouin scattering process demonstrated here, a pump photon of frequency ω_p is scattered into a lower-frequency counter-propagating Stokes photon at ω_s, and a forward-travelling acoustic phonon of frequency Ω_B and wavelength λ_B in the superfluid, where energy and momentum conservation dictate that $\omega_p = \omega_s + \Omega_B$ and that the optical wavelength $\lambda_{light} = 2\lambda_B$ (Fig. 1a). In solids, the deformation due to electrostriction is determined by the Young's modulus, E. By contrast, in our experiments, regions of high light intensity inside the resonator continuously deform a fluid interface by drawing in more superfluid by means of an optical gradient force and the superfluid fountain effect[31,33]. Here, the equivalent of the Young's modulus is the van der Waals pressure on the surface of the fluid, $P_v = 3\alpha_v\rho/d^3$, where α_v is the van der Waals coefficient, ρ is the fluid density and d is its thickness. While both electrostriction and surface deformation result in a periodically modulated refractive index grating that scatters pump light (illustrated for our case in Fig. 1d), for typical few-nanometre-thick films the van der Waals pressure is over six orders of magnitude lower than the Young's modulus of typical Brillouin-active solids (~kPa versus GPa). As a result, the modulation achieved per photon can be much larger, enabling the ultralow-threshold lasing reported here, and providing the future prospect to reach quantum regimes. The reduced stiffness greatly reduces the speed of sound c, from kilometres per second for solids to metres per second for superfluid films. This results in a Brillouin shift $\Omega_B/2\pi = 2c/\lambda_{light}$ in the megahertz

[1]ARC Centre of Excellence for Engineered Quantum Systems, The University of Queensland, St Lucia, Queensland, Australia. [2]These authors contributed equally: Xin He, Glen I. Harris, Christopher G. Baker. *e-mail: c.baker3@uq.edu.au

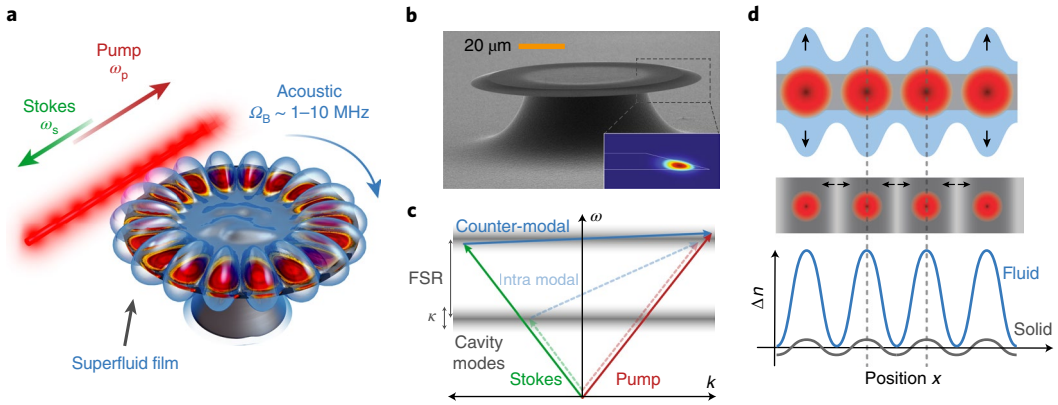

Fig. 1 | Brillouin scattering with compliant fluid interfaces. a, Illustration of the backward Brillouin scattering process in the superfluid optomechanical resonator. Arrows indicate the direction of pump photons (red), Stokes photons (green) and acoustic phonons (blue). **b**, Top: scanning electron microscope image of a silica microdisc resonator on the silicon chip (radius 40 μm, thickness 2 μm). Inset: cross-section showing the electric field norm of a quasi-TE (transverse electric) mode supported by the microdisc. **c**, Dispersion diagram showing the energy and momentum matching conditions for the Stokes interaction; shaded horizontal bands represent the increased density of states of cavity modes. Conventional intramodal Brillouin scattering (dashed lines) typically leverages optical modes separated by a free spectral range (FSR) or multiple thereof, limiting device sizes to millimetre scales. The scattering between degenerate, counter-propagating whispering gallery modes of equivalent azimuthal order m observed here overcomes this limitation, and is referred to as counter-modal (solid lines). **d**, Schematic illustration of the Brillouin interaction in our superfluid system (top) and in a solid material where the optical field is responsible for compression and rarefaction of the medium (middle). Due to threefold resonant enhancement, the optically driven refractive index modulation (bottom) is larger in the fluid case.

range, versus the gigahertz range in many solids at telecommunication wavelengths.

These unique features offer two advantages. First, because of the small frequency shift, the Stokes beam is naturally resonant with the degenerate whispering gallery mode that counter-propagates with the pump mode, as depicted in Fig. 1c (solid lines) and referred to here as counter-modal Brillouin scattering. This alleviates the need for potentially complex spectral engineering of the resonator[14,22] and allows resonant enhancement that is independent of the device size, down to mode volumes in the range of the optical wavelength cubed. While such miniaturization is desirable as it enhances the strength of the Brillouin interaction, it has so far been hampered in conventional backward intramodal scattering[34] by the inability to meet momentum and energy conservation criteria in micrometre-scale devices whose free spectral range far exceeds the Brillouin shift (Fig. 1c, dashed lines). Second, and a key result of this work, the strong Brillouin scattering enables the emergence of mechanically mediated strong optical coupling, hybridizing the initially degenerate forward and backward propagating fields.

The optical pumping of phonons into the forward travelling acoustic wave in backward Brillouin scattering amplifies the acoustic wave, modifying its linewidth to

$$\Gamma_{\mathrm{eff}} = \Gamma - \frac{4g_{0,\mathrm{tot}}g_{0,\mathrm{rp}}}{\kappa}\,\zeta n_{\mathrm{cav}} \qquad (1)$$

where Γ is the intrinsic linewidth, n_{cav} is the intracavity photon number, κ is the loaded optical linewidth and $g_{0,\mathrm{tot}} = g_{0,\mathrm{rp}} + g_{0,\mathrm{fp}}$ is the single-photon optomechanical coupling rate, which includes radiation-pressure ($g_{0,\mathrm{rp}}$) and fountain-pressure ($g_{0,\mathrm{fp}}$) components (Supplementary Information). The parameter $\zeta < 1$ quantifies a reduction in Brillouin amplification from the presence of optical backscattering, caused by geometric imperfections of the microdisc. This reduction is due both to the backscattering-induced depletion of the pump field and to active cooling of the acoustic mode by the backscattered photons, which directly competes with the amplification from the pump. Once the effective linewidth crosses zero, the acoustic damping is offset by the Brillouin amplification. In this regime, spontaneously occurring thermal excitations in the superfluid film are exponentially amplified to a large coherent amplitude, that is, the system exhibits phonon lasing.

This process is analogous to parametric amplification in cavity optomechanics. Indeed, there has been recent theoretical interest in unifying the fields of cavity optomechanics and Brillouin scattering[35,36], which have traditionally referred to standing-wave and travelling-wave interactions, respectively. As discussed below, in our system it is possible to transition between these two scenarios in situ, within the same device.

The apparatus used to experimentally probe these two regimes and demonstrate superfluid thin-film Brillouin lasing is shown in Fig. 2, with details given in Methods. Tuning the position of the coupling fibre taper mediates a transition from a standing- to a travelling-wave interaction, enabled by a small amount of optical backscattering (see Supplementary Information for more information). This transition manifests in the optical power spectrum as symmetric (Fig. 3a top) and asymmetric (Fig. 3a bottom) optical sidebands, which correspond to the optomechanical and Brillouin regimes,

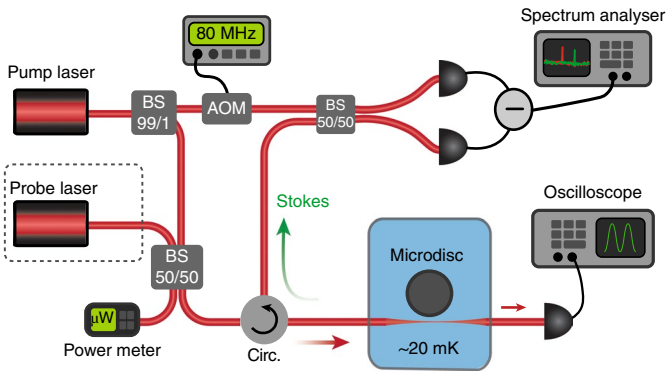

Fig. 2 | Schematic of the experimental set-up. BS, beamsplitter; AOM, acousto-optic modulator; blue box, sample chamber in the dilution refrigerator; Circ., optical circulator. Arrows represent pump photons (red) and Stokes photons (green).

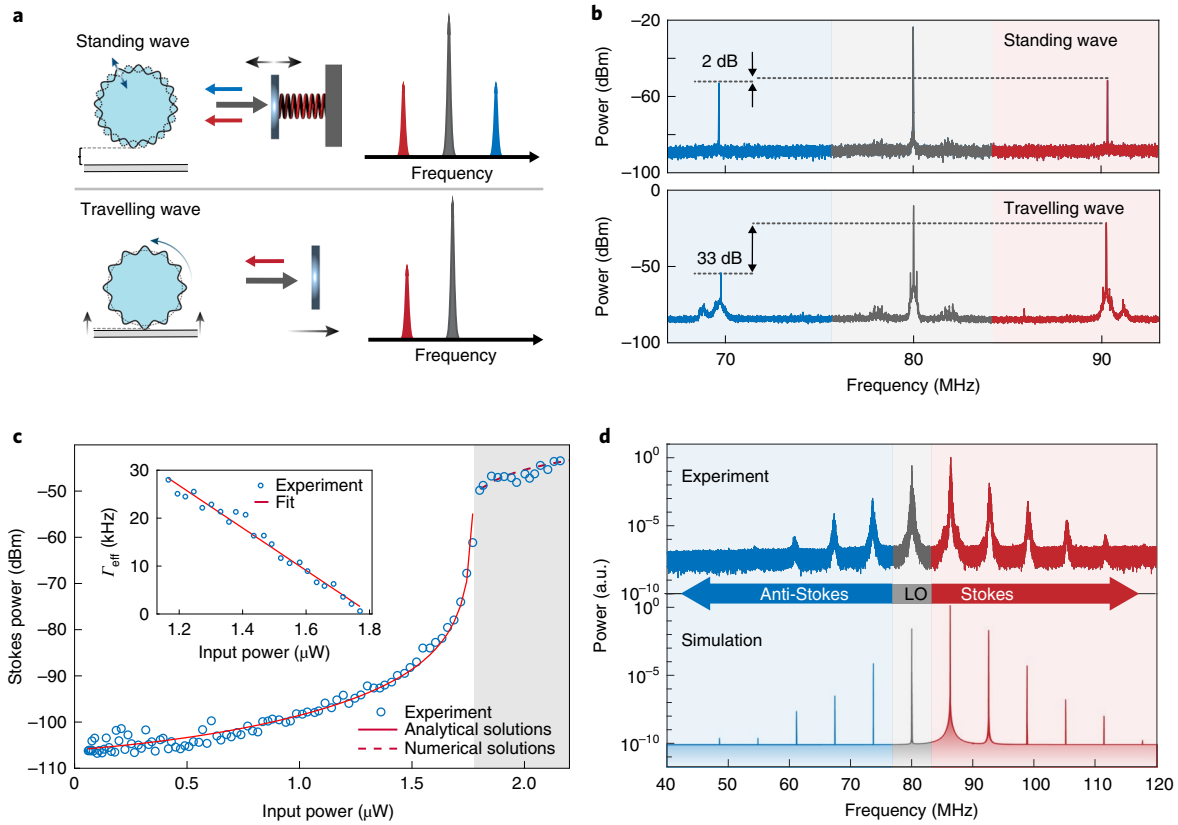

Fig. 3 | Tuning from standing-wave optomechanics to travelling-wave Brillouin lasing. a, Illustration of the different optical power spectra obtained after a pump beam interacts with a standing-wave (top) or travelling-wave (bottom) acoustic mode. These two situations can be experimentally accessed simply by tuning the taper–microdisc separation (Methods and Supplementary Information). **b**, As the taper–microdisc separation is decreased the optical power spectrum exhibits increased sideband asymmetry, verifying the standing-wave (top) or travelling-wave (bottom) nature of the interaction. **c**, Stokes sideband peak power versus input laser power (blue circles). The solid red line is an analytical fit to the data in the non-depleted pump regime; the dashed red line is a fit obtained by numerically solving the full equations of motion (Methods and Supplementary Information). The shaded region above 1.8 μW marks the onset of Brillouin lasing. Inset: Γ_{eff} versus input power, along with fit by equation (1). **d**, Brillouin lasing spectra measured at 5.6 μW input power (top, experimental spectrum; bottom, numerical solution to theory). LO (grey shading): peak due to beat between pump and heterodyne local oscillator. Note that the experiment and theory deviate within this region due to additional backscattering of the pump that is not present in the simulation (Supplementary Information). Stokes sidebands appear at higher frequencies due to the heterodyne detection.

respectively. This is experimentally demonstrated in Fig. 3b, which shows an increase in sideband asymmetry of approximately 31 dB on transitioning from a standing- to a travelling-wave scenario.

Hereafter, we consider only the situation of travelling acoustic waves (that is Brillouin scattering). Figure 3c shows the observed Stokes signal peak power as a function of input laser power for $\Omega_{\mathrm{B}}=7.3$ MHz, while the inset shows the Stokes linewidth versus power. As can be seen, the Stokes wave is amplified with increasing input power in good agreement with theory, and crosses the threshold to lasing at a power of 1.8 μW. Fitting the linewidth data to equation (1) yields an intrinsic acoustic linewidth of $\Gamma/2\pi=85\pm6$ kHz. We extract a total single-photon coupling rate of $g_{0,\mathrm{tot}}/2\pi=133$ kHz, independently of ζ, through numerical simulations that include all dynamic couplings between optical and acoustic modes induced by backscattering. The radiation-pressure component is estimated to be $g_{0,\mathrm{rp}}/2\pi=11$ kHz from finite-element modelling (Supplementary Information), leaving a fountain-pressure contribution of $g_{0,\mathrm{fp}}/2\pi=122$ kHz. The total single-photon coupling rate is more than three orders of magnitude larger than that achieved using the electrostrictive interaction in similar-sized silica microspheres[29]. Furthermore, it represents a several-order-of-magnitude increase compared with previous superfluid optomechanics experiments with microtoroidal cavities[15,27,31]. The fountain pressure is introduced by optical heating through the temperature dependence of the entropy of the film. Gradients in entropy induce a flow of the superfluid component in an analogous manner to optical gradient forces. Despite the observed strength of this interaction, we verify that it comes in concert with only minimal levels of bulk heating, and with feasible modifications could allow ground-state cooling[37,38] (Supplementary Information).

Above the lasing threshold the pump light is depleted by scattering off the strong superfluid travelling refractive index grating, such that the linearized theory is no longer valid. Furthermore, the presence of optical backscattering introduces a dynamic coupling between optical modes. Therefore, the above-threshold behaviour is fitted by numerically solving the full equations of motion of the optical and acoustic fields (Supplementary Information). These simulations are in good agreement with both the measured power scaling (dashed red curve in Fig. 3c) and the optical power spectra (Fig. 3d), providing a confirmation of the saturation behaviour through pump depletion. It should be noted that the multiple Stokes lines seen in Fig. 3d arise due to a combination of nonlinear mixing, which is mediated by optical backscattering, and higher-order Stokes scattering (see Supplementary Information for more details).

In the Brillouin interaction, the lasing of the copropagating acoustic wave creates an effective refractive index grating travelling

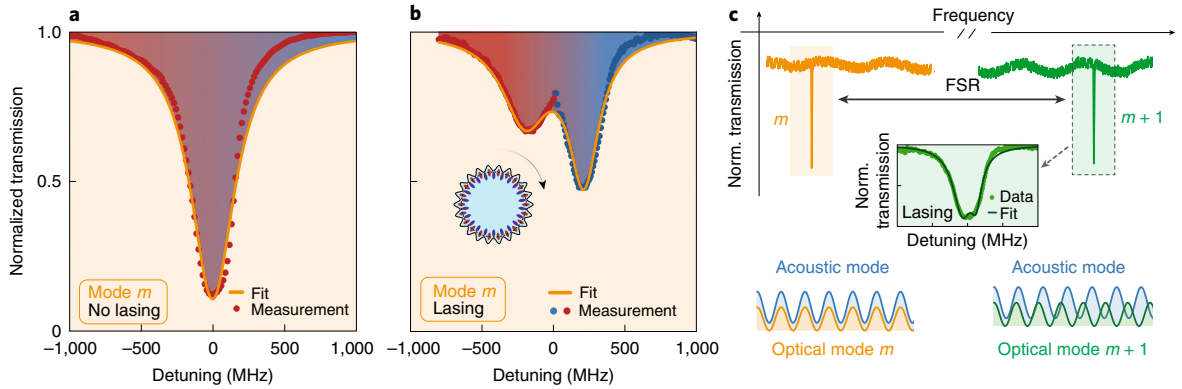

Fig. 4 | Strong phonon-mediated optical coupling. a, With the pump laser off, the optical doublet measured by the probe beam is degenerate. **b**, At 5.1 μW pump power, the lasing of the Brillouin wave splits the modes into a resolvable doublet. **c**, Optical spectrum showing two optical modes separated by an FSR (top). Inset: mode $m+1$ (green) remains degenerate, even in the presence of a strong pump applied to mode m (orange). The orthogonality between modes m and $m+1$ is illustrated by the overlap between surface deformation and optical intensity.

at the speed of sound. If the backscattering generated from this grating is sufficiently strong, it is possible to enter a regime of mechanically mediated photon–photon strong coupling, where photons cycle between the pump and Stokes resonances at a rate faster than the decay rate of the optical fields. This should be distinguished from the phonon–photon strong coupling previously demonstrated in both conventional[39] and Brillouin[22] optomechanics. The signature of this strong coupling is that the pump and Stokes resonances hybridize into a new pair of frequency-shifted optical eigenmodes, with frequencies given by

$$\omega_{\pm} = \bar{\omega} \pm \sqrt{\Omega_B^2/4 + g_{opt}^2} \quad (2)$$

where $\bar{\omega} = (\omega_p + \omega_s)/2$ is the average of the two bare optical modes that support the pump and Stokes photons, and $g_{opt} = g_{0,rp}\beta$ is the phonon-boosted optomechanical coupling rate with β the amplitude of the copropagating acoustic wave (Supplementary Information).

Our superfluid thin-film optomechanical Brillouin laser is naturally suited to observe the mode hybridization induced by strong coupling due to its combination of high $g_{0,rp}$ and low Ω_B. This allows access to the regime where $g_{opt} \gg \Omega_B$, in which the optical modes are shifted by frequencies of $\pm\left[(\Omega_B^2/4 + g_{opt}^2)^{1/2} - \Omega_B/2\right] \sim \pm g_{opt}$. By comparison, in the usual regime, where the Brillouin frequency is high enough that $\Omega_B \gg g_{opt}$, the optical mode shifts are suppressed by a factor of Ω_B/g_{opt}.

To spectroscopically explore the regime of strong coupling we implement a pump–probe measurement scheme, shown in Fig. 2 and described in Methods. Figure 4 shows the optical resonance measured with this set-up. With the pump laser off (Fig. 4a), no splitting is evident between the clockwise (pump) and anticlockwise (Stokes) optical modes. Injecting 5 μW of pump light initiates spontaneous Brillouin lasing, as verified through the reflected light power spectrum. Due to the high-contrast refractive index grating generated by the Brillouin lasing process, two distinct non-degenerate cavity resonances can now be resolved (Fig. 4b): a lower-frequency resonance (red) sensing the peaks of the superfluid Brillouin wave, and a higher-frequency resonance (blue)—spatially shifted by $\lambda_B/2$—sensing the troughs; see the inset of Fig. 4b and Supplementary Information. The magnitude of the splitting provides $g_{opt} = 2\pi \times 187$ MHz, which is larger than the half-width at half-maximum of the optical mode ($\kappa/2 = 2\pi \times 142$ MHz), indicating mechanically mediated strong coupling between the two optical modes[39].

It should be noted that the increase in optical linewidth of the lower-frequency hybrid mode, observed in Fig. 4b, is not always a feature of strong coupling. We ascribe this feature to a preferential increase in scattering to free-space modes, mediated by the dielectric protrusions created by large superfluid deformations. Indeed, this effect is well known in the context of nanoparticle detection using high-Q (optical quality factor) whispering gallery modes[40].

A key feature of Brillouin scattering is the unique acoustic wave that links the pump and Stokes fields. Since whispering gallery modes constitute orthogonal eigenmodes of the electromagnetic field, the superfluid surface deformation caused by driving one whispering gallery mode should leave other whispering gallery modes unaffected. Indeed, we verify that the adjacent whispering gallery mode (mode $m+1$, Fig. 4c (green colour)) is unaffected by the refractive index grating responsible for the strong coupling observed on mode m (Fig. 4b,c (orange colour)). This orthogonality of the Brillouin grating is schematically illustrated in the lower section of Fig. 4c (see Supplementary Information for more details).

In summary, we have shown that optically induced surface deformations in liquids can facilitate greatly enhanced Brillouin interactions. We use this concept to demonstrate ultralow-threshold Brillouin lasing in few-nanometre-thick superfluid helium films and, for the first time, phonon-mediated strong coupling between optical cavity modes. The microwatt-range lasing threshold presented here is lower than previously reported values[41–43], albeit at orders-of-magnitude lower frequency and achieved using an approach that is not directly comparable. Furthermore, even modest improvements in acoustic dissipation and optical linewidth—achieved for example by reducing sidewall roughness on our existing devices[42]—could lower the threshold power into the picowatt range, well below what can be achieved with solid-state systems.

The system presented here represents a substantial departure from traditional travelling-wave Brillouin systems, which typically exhibit weak single-photon coupling due to large mode volumes and high Young's moduli. While this can be partially mitigated via resonant enhancement, doing so typically requires millimetre-scale devices to satisfy energy and momentum matching requirements[2,14]. In contrast, superfluid helium, with its ultracompliant fluid interface, affords a low-frequency Brillouin shift that is naturally resonant with the counter-propagating whispering gallery mode, regardless of the device size. This paves the way towards resonantly enhanced backward Brillouin scattering on devices with mode volumes as small as the optical wavelength cubed and with optomechanical coupling rates in excess of $g_{0,rp}/2\pi \sim 300$ kHz[28].

Phonon lasing in superfluid helium opens up a new approach to explore quantum turbulence and quantum fluid dynamics in a

strongly interacting system[15]. In this application, the combination of phonon-laser-induced mechanical line narrowing[44] with operation as a precision Brillouin gyroscope[14] would provide unprecedented sensitivity in measurements of the quantized circulation of the superfluid. Applied to conventional fluids, the same Brillouin process could be used to optically mix microdroplets and to probe their material properties, important tools for picolitre-scale chemistry, biophysics and the biosciences[45,46]. Moreover, strong phonon-mediated optical coupling may allow the generation of synthetic electromagnetic fields[12,13], and superfluid-based optical switches and reconfigurable optical circuits[9,10].

Online content

Any methods, additional references, Nature Research reporting summaries, source data, extended data, supplementary information, acknowledgements, peer review information; details of author contributions and competing interests; and statements of data and code availability are available at https://doi.org/10.1038/s41567-020-0785-0.

Received: 15 July 2019; Accepted: 2 January 2020;
Published online: 10 February 2020

References

1. Kittlaus, E. A., Otterstrom, N. T. & Rakich, P. T. On-chip inter-modal Brillouin scattering. *Nat. Commun.* **8**, 15819 (2017).
2. Li, J., Lee, H. & Vahala, K. J. Microwave synthesizer using an on-chip Brillouin oscillator. *Nat. Commun.* **4**, 2097 (2013).
3. Eggleton, B. J., Poulton, C. G. & Pant, R. Inducing and harnessing stimulated Brillouin scattering in photonic integrated circuits. *Adv. Opt. Photon.* **5**, 536–587 (2013).
4. Scarcelli, G. & Yun, S. H. Confocal Brillouin microscopy for three-dimensional mechanical imaging. *Nat. Photon.* **2**, 39–43 (2008).
5. Renninger, W. H., Kharel, P., Behunin, R. O. & Rakich, P. T. Bulk crystalline optomechanics. *Nat. Phys.* **14**, 601–607 (2018).
6. Kharel, P. et al. High-frequency cavity optomechanics using bulk acoustic phonons. *Sci. Adv.* **5**, eaav0582 (2019).
7. Kashkanova, A. D. et al. Superfluid Brillouin optomechanics. *Nat. Phys.* **13**, 74–79 (2017).
8. Giorgini, A. et al. Stimulated Brillouin cavity optomechanics in liquid droplets. *Phys. Rev. Lett.* **120**, 073902 (2018).
9. Ruesink, F., Mathew, J. P., Miri, M.-A., Alù, A. & Verhagen, E. Optical circulation in a multimode optomechanical resonator. *Nat. Commun.* **9**, 1798 (2018).
10. Shen, Z. et al. Reconfigurable optomechanical circulator and directional amplifier. *Nat. Commun.* **9**, 1797 (2018).
11. Safavi-Naeini, A. H. & Painter, O. Proposal for an optomechanical traveling wave phonon–photon translator. *New J. Phys.* **13**, 013017 (2011).
12. Fang, K. et al. Generalized non-reciprocity in an optomechanical circuit via synthetic magnetism and reservoir engineering. *Nat. Phys.* **13**, 465–471 (2017).
13. Schmidt, M., Kessler, S., Peano, V., Painter, O. & Marquardt, F. Optomechanical creation of magnetic fields for photons on a lattice. *Optica* **2**, 635–641 (2015).
14. Li, J., Suh, M. & Vahala, K. Microresonator Brillouin gyroscope. *Optica* **4**, 346–348 (2017).
15. Sachkou, Y. P. et al. Coherent vortex dynamics in a strongly interacting superfluid on a silicon chip. *Science* **366**, 1480–1485 (2019).
16. Gauthier, G. et al. Giant vortex clusters in a two-dimensional quantum fluid. *Science* **364**, 1264–1267 (2019).
17. Reinke, C., Rakich, P. T., Wang, Z., Camacho, R. & Davids, P. Giant enhancement of stimulated Brillouin scattering in the subwavelength limit. *Phys. Rev. X* **2**, 011008 (2012).
18. Kittlaus, E. A., Shin, H. & Rakich, P. T. Large Brillouin amplification in silicon. *Nat. Photon.* **10**, 463–467 (2016).
19. Florez, O. et al. Brillouin scattering self-cancellation. *Nat. Commun.* **7**, 11759 (2016).
20. Van Laer, R., Kuyken, B., Van Thourhout, D. & Baets, R. Interaction between light and highly confined hypersound in a silicon photonic nanowire. *Nat. Photon.* **9**, 199–203 (2015).
21. Shin, H. et al. Tailorable stimulated Brillouin scattering in nanoscale silicon waveguides. *Nat. Commun.* **4**, 1944 (2013).
22. Enzian, G. et al. Observation of Brillouin optomechanical strong coupling with an 11 GHz mechanical mode. *Optica* **6**, 7–14 (2019).
23. Gundavarapu, S. et al. Sub-hertz fundamental linewidth photonic integrated Brillouin laser. *Nat. Photon.* **13**, 60–67 (2019).
24. Dong, C. H. et al. Brillouin-scattering-induced transparency and non-reciprocal light storage. *Nat. Commun.* **6**, 6193 (2015).
25. Wolff, C., Steel, M. J., Eggleton, B. J. & Poulton, C. G. Stimulated Brillouin scattering in integrated photonic waveguides: forces, scattering mechanisms, and coupled-mode analysis. *Phys. Rev. A* **92**, 013836 (2015).
26. Kaminski, S., Martin, L. L., Maayani, S. & Carmon, T. Ripplon laser through stimulated emission mediated by water waves. *Nat. Photon.* **10**, 758–761 (2016).
27. Harris, G. I. et al. Laser cooling and control of excitations in superfluid helium. *Nat. Phys.* **12**, 788–793 (2016).
28. Baker, C. G. et al. Theoretical framework for thin film superfluid optomechanics: towards the quantum regime. *New J. Phys.* **18**, 123025 (2016).
29. Bahl, G., Tomes, M., Marquardt, F. & Carmon, T. Observation of spontaneous Brillouin cooling. *Nat. Phys.* **8**, 203–207 (2012).
30. Bahl, G. et al. Brillouin cavity optomechanics with microfluidic devices. *Nat. Commun.* **4**, 2994 (2013).
31. McAuslan, D. L. et al. Microphotonic forces from superfluid flow. *Phys. Rev. X* **6**, 021012 (2016).
32. Atkins, K. R. Third and fourth sound in liquid helium II. *Phys. Rev.* **113**, 962–965 (1959).
33. Ashkin, A., Dziedzic, J. M., Bjorkholm, J. E. & Chu, S. Observation of a single-beam gradient force optical trap for dielectric particles. *Opt. Lett.* **11**, 288–290 (1986).
34. Wiederhecker, G. S., Dainese, P. & MayerAlegre, T. P. Brillouin optomechanics in nanophotonic structures. *APL Photon.* **4**, 071101 (2019).
35. Rakich, P. & Marquardt, F. Quantum theory of continuum optomechanics. *New J. Phys.* **20**, 045005 (2018).
36. Van Laer, R., Baets, R. & Van Thourhout, D. Unifying Brillouin scattering and cavity optomechanics. *Phys. Rev. A* **93**, 053828 (2016).
37. Metzger, C. H. & Karrai, K. Cavity cooling of a microlever. *Nature* **432**, 1002–1005 (2004).
38. Jourdan, G., Comin, F. & Chevrier, J. Mechanical mode dependence of bolometric backaction in an atomic force microscopy microlever. *Phys. Rev. Lett.* **101**, 133904 (2008).
39. Verhagen, E., Deleglise, S., Weis, S., Schliesser, A. & Kippenberg, T. J. Quantum-coherent coupling of a mechanical oscillator to an optical cavity mode. *Nature* **482**, 63–67 (2012).
40. Zhu, J. et al. On-chip single nanoparticle detection and sizing by mode splitting in an ultrahigh- *Q* microresonator. *Nat. Photon.* **4**, 46–49 (2010).
41. Grudinin, I. S., Matsko, A. B. & Maleki, L. Brillouin lasing with a CaF_2 whispering gallery mode resonator. *Phys. Rev. Lett.* **102**, 043902 (2009).
42. Lee, H. et al. Chemically etched ultrahigh- Q wedge-resonator on a silicon chip. *Nat. Photon.* **6**, 369–373 (2012).
43. Guo, C. et al. Ultralow-threshold cascaded Brillouin microlaser for tunable microwave generation. *Opt. Lett.* **40**, 4971–4974 (2015).
44. Feng, X. L., White, C. J., Hajimiri, A. & Roukes, M. L. A self-sustaining ultrahigh-frequency nanoelectromechanical oscillator. *Nat. Nanotechnol.* **3**, 342–346 (2008).
45. Destgeer, G. & Sung, H. J. Recent advances in microfluidic actuation and micro-object manipulation via surface acoustic waves. *Lab Chip* **15**, 2722–2738 (2015).
46. Palombo, F. & Fioretto, D. Brillouin light scattering: applications in biomedical sciences. *Chem. Rev.* **119**, 7833–7847 (2019).

Methods

Experimental apparatus used to probe superfluid Brillouin lasing. To experimentally probe superfluid thin-film Brillouin lasing, we employ the experimental apparatus shown in Fig. 2. The microdisc is coupled to a tapered fibre and cooled to ~20 mK in a sealed sample chamber within a dilution refrigerator. Helium-4 gas injected into the chamber forms a nanometre-thick self-assembling superfluid film coating the microresonator[27] (Supplementary Information). A telecommunication-wavelength pump laser drives the Brillouin lasing process, and the backwards emitted Stokes and anti-Stokes light is observed using optical heterodyne detection (80 MHz shifted local oscillator) and characterized on a spectrum analyser. We select a microdisc optical mode at $\lambda_{light} = 1{,}555$ nm with a loaded linewidth of $\kappa/2\pi = 284$ MHz, corresponding to $Q \simeq 7 \times 10^5$. This optical mode is also found to have a backscattering rate of $\kappa/2\pi = 75$ MHz which suppresses the Brillouin-induced linewidth narrowing by a factor of $\zeta = 0.22$ (equation (1) and Supplementary Information).

Pump–probe scheme used to characterize phonon-mediated strong coupling. To spectroscopically characterize phonon-mediated strong coupling, a weak tunable diode probe laser is added to the heterodyne set-up shown in Fig. 2. While the pump laser is set on resonance with the optical mode, the probe laser is repeatedly swept at 100 Hz across the optical resonance. The transmitted optical photodetector signal is low-pass filtered (filter bandwidth = 20 kHz) and averaged 256 times on an oscilloscope to obtain the optical cavity spectrum, free from any potential modulation due to the Brillouin lasing process.

Data availability

The data represented in Figs. 3b–d and 4 are available as Source Data. All other data that support the plots within this paper and other findings of this study are available from the corresponding author on reasonable request.

Code availability

All relevant codes or algorithms are available from the corresponding author on reasonable request.

Acknowledgements

This work was funded by the US Army Research Office through grant number W911NF17-1-0310 and the Australian Research Council Centre of Excellence for Engineered Quantum Systems (EQUS, project number CE170100009). W.P.B. and C.G.B respectively acknowledge Australian Research Council Fellowships FT140100650 and DE190100318. This work was performed in part at the Queensland node of the Australian National Fabrication Facility, a company established under the National Collaborative Research Infrastructure Strategy to provide nano- and microfabrication facilities for Australia's researchers.

Author contributions

X.H., G.I.H., C.G.B., A.S. and Y.L.S. collected the data. X.H., G.I.H., C.G.B., A.S., Y.L.S. and W.P.B. performed the data analysis and developed the theory. X.H., G.I.H., C.G.B., A.S., Y.L.S., Y.P.S. and S.F. contributed to device fabrication and building the experimental set-up. C.G.B. and W.P.B. conceived the idea. All authors contributed to the manuscript. W.P.B. led the project with assistance from C.G.B. and G.I.H.

Competing interests

The authors declare no competing interests.

Additional information

Supplementary information is available for this paper at https://doi.org/10.1038/s41567-020-0785-0.

Correspondence and requests for materials should be addressed to C.G.B.

Peer review information *Nature Physics* thanks Tal Carmon and Gustavo Wiederhecker for their contribution to the peer review of this work.